Optical Materials EXPRESS

MoS_2 saturable absorber for passive Q-switching of Yb and Tm microchip lasers

JOSEP MARIA SERRES,[1] PAVEL LOIKO,[1,2] XAVIER MATEOS,[1,3,6,*] HAOHAI YU,[4] HUAIJIN ZHANG,[4] YANXUE CHEN,[5] VALENTIN PETROV,[2] UWE GRIEBNER,[2] KONSTANTIN YUMASHEV,[3] MAGDALENA AGUILÓ,[1] AND FRANCESC DÍAZ[1]

[1] *Física i Cristal·lografia de Materials i Nanomaterials (FiCMA-FiCNA), Universitat Rovira i Virgili (URV), Campus Sescelades, c/ Marcel·lí Domingo, s/n., E-43007 Tarragona, Spain*
[2] *Center for Optical Materials and Technologies (COMT), Belarusian National Technical University, 65/17 Nezavisimosti Ave., 220013 Minsk, Belarus*
[3] *Max Born Institute for Nonlinear Optics and Short Pulse Spectroscopy, Max-Born-Str. 2A, D-12489 Berlin, Germany*
[4] *State Key Laboratory of Crystal Materials and Institute of Crystal Materials, Shandong University, 250100 Jinan, China*
[5] *School of Physics, Shandong University, 250100 Jinan, China*
[6] *xavier.mateos@urv.cat*
[*] *mateos@mbi-berlin.de*

Abstract: A multi-layer MoS_2-based saturable absorber (SA) enables Q-switched operation of Yb and Tm microchip lasers. The saturation intensity of MoS_2-SA is determined to be about ~0.5 MW/cm^2. The Q-switched Tm laser generated 1.27 W at 1929 nm with a slope efficiency of 43% and conversion efficiency with respect to the continuous-wave mode as high as 81%. The pulse characteristics were 175 ns / 7.5 µJ corresponding to a repetition rate of 170 kHz. With the Q-switched Yb laser, 220 ns / 0.5 µJ pulses were achieved at 1030 nm. We show that using MoS_2-SA at ~2 µm is advantageous as compared to multi-layer graphene. We also prove that MoS_2-SA is more efficient at ~2 µm compared to ~1 µm due to a lower saturation intensity and higher fraction of the saturable loss.

OCIS codes: (160.4330) Nonlinear optical materials; (140.3540) Lasers, Q-switched.

References and links

1. C. Ataca, H. Şahin, and S. Ciraci, “Stable, single-layer MX_2 transition-metal oxides and dichalcogenides in a honeycomb-like structure,” J. Phys. Chem. C **116**(16), 8983–8999 (2012).
2. A. F. Wells, Structural Inorganic Chemistry (Clarendon Press, Oxford, 1984).
3. K. F. Mak, C. Lee, J. Hone, J. Shan, and T. F. Heinz, “Atomically thin MoS_2: a new direct-gap semiconductor,” Phys. Rev. Lett. **105**(13), 136805 (2010).
4. A. Splendiani, L. Sun, Y. Zhang, T. Li, J. Kim, C.-Y. Chim, G. Galli, and F. Wang, “Emerging photoluminescence in monolayer MoS_2,” Nano Lett. **10**(4), 1271–1275 (2010).
5. K. He, C. Poole, K. F. Mak, and J. Shan, “Experimental demonstration of continuous electronic structure tuning via strain in atomically thin MoS_2,” Nano Lett. **13**(6), 2931–2936 (2013).
6. S. Wang, H. Yu, H. Zhang, A. Wang, M. Zhao, Y. Chen, L. Mei, and J. Wang, “Broadband few-layer MoS_2 saturable absorbers,” Adv. Mater. **26**(21), 3538–3544 (2014).
7. R. R. Nair, P. Blake, A. N. Grigorenko, K. S. Novoselov, T. J. Booth, T. Stauber, N. M. R. Peres, and A. K. Geim, “Fine structure constant defines visual transparency of graphene,” Science **320**(5881), 1308 (2008).
8. H. Zhang, S. B. Lu, J. Zheng, J. Du, S. C. Wen, D. Y. Tang, and K. P. Loh, “Molybdenum disulfide (MoS_2) as a broadband saturable absorber for ultra-fast photonics,” Opt. Express **22**(6), 7249–7260 (2014).
9. K. Wang, J. Wang, J. Fan, M. Lotya, A. O’Neill, D. Fox, Y. Feng, X. Zhang, B. Jiang, Q. Zhao, H. Zhang, J. N. Coleman, L. Zhang, and W. J. Blau, “Ultrafast saturable absorption of two-dimensional MoS_2 nanosheets,” ACS Nano **7**(10), 9260–9267 (2013).
10. H. Zhang, D. Y. Tang, L. M. Zhao, Q. L. Bao, and K. P. Loh, “Large energy mode locking of an erbium-doped fiber laser with atomic layer graphene,” Opt. Express **17**(20), 17630–17635 (2009).
11. S. B. Lu, L. L. Miao, Z. N. Guo, X. Qi, C. J. Zhao, H. Zhang, S. C. Wen, D. Y. Tang, and D. Y. Fan, “Broadband nonlinear optical response in multi-layer black phosphorus: an emerging infrared and mid-infrared optical material,” Opt. Express **23**(9), 11183–11194 (2015).

#270951 http://dx.doi.org/10.1364/OME.6.003262
Journal © 2016 Received 21 Jul 2016; revised 5 Sep 2016; accepted 9 Sep 2016; published 26 Sep 2016

12. Z. Luo, Y. Huang, M. Zhong, Y. Li, J. Wu, B. Xu, H. Xu, Z. Cai, J. Peng, and J. Weng, "1-, 1.5-, and 2-μm fiber lasers Q-switched by a broadband few-layer MoS$_2$ saturable absorber," J. Lightwave Technol. **32**(24), 4679–4686 (2014).
13. J. Du, Q. Wang, G. Jiang, C. Xu, C. Zhao, Y. Xiang, Y. Chen, S. Wen, and H. Zhang, "Ytterbium-doped fiber laser passively mode locked by few-layer Molybdenum Disulfide (MoS$_2$) saturable absorber functioned with evanescent field interaction," Sci. Rep. **4**, 6346 (2014).
14. Y. Zhang, S. Wang, D. Wang, H. Yu, H. Zhang, Y. Chen, L. Mei, A. Di Lieto, M. Tonelli, and J. Wang, "Atomic-layer molybdenum sulphide passively modulated green laser pulses," IEEE Photonics Technol. Lett. **28**(2), 197–200 (2016).
15. Y. Sun, J. Xu, S. Gao, C. Lee, H. Xia, Y. Wang, Z. You, and C. Tu, "Wavelength-tunable, passively Q-switched Yb^{3+}:Ca$_3$Y$_2$(BO$_3$)$_4$ solid-state laser using MoS$_2$ saturable absorber," Mater. Lett. **160**, 268–270 (2015).
16. F. Lou, R. Zhao, J. He, Z. Jia, X. Su, Z. Wang, J. Hou, and B. Zhang, "Nanosecond-pulsed, dual-wavelength, passively Q-switched ytterbium-doped bulk laser based on few-layer MoS$_2$ saturable absorber," Photon. Res. **3**(2), A25–A29 (2015).
17. B. Xu, Y. Cheng, Y. Wang, Y. Huang, J. Peng, Z. Luo, H. Xu, Z. Cai, J. Weng, and R. Moncorgé, "Passively Q-switched Nd:YAlO$_3$nanosecond laser using MoS$_2$as saturable absorber," Opt. Express **22**(23), 28934–28940 (2014).
18. P. Ge, J. Liu, S. Jiang, Y. Xu, and B. Man, "Compact Q-switched 2 μm Tm:GdVO$_4$ laser with MoS$_2$ absorber," Photon. Res. **3**(5), 256–259 (2015).
19. J. M. Serres, P. Loiko, X. Mateos, K. Yumashev, U. Griebner, V. Petrov, M. Aguiló, and F. Díaz, "Tm:KLu(WO$_4$)$_2$ microchip laser Q-switched by a graphene-based saturable absorber," Opt. Express **23**(11), 14108–14113 (2015).
20. T. Zhao, Y. Wang, H. Chen, and D. Shen, "Graphene passively Q-switched Ho:YAG ceramic laser," Appl. Phys. B **116**(4), 947–950 (2014).
21. R. Lan, P. Loiko, X. Mateos, Y. Wang, J. Li, Y. Pan, S. Y. Choi, M. H. Kim, F. Rotermund, A. Yasukevich, K. Yumashev, U. Griebner, and V. Petrov, "Passive Q-switching of microchip lasers based on Ho:YAG ceramic," Appl. Opt. in press.
22. T. L. Feng, S. Z. Zhao, K. J. Yang, G. Q. Li, D. C. Li, J. Zhao, W. C. Qiao, L. H. Zheng, J. Xu, G. J. Zhao, and Y. G. Wang, "A diode-pumped passively Q-switched Tm,Ho:YAP laser with a single-walled carbon nanotube," Laser Phys. Lett. **10**(9), 095001 (2013).
23. J. J. Zayhowski and C. Dill Iii, "Diode-pumped passively Q-switched picosecond microchip lasers," Opt. Lett. **19**(18), 1427–1429 (1994).
24. N. T. McDevitt, J. S. Zabinski, M. S. Donley, and J. E. Bultman, "Disorder-induced low-frequency Raman band observed in deposited MoS$_2$ films," Appl. Spectrosc. **48**(6), 733–736 (1994).
25. J. M. Serres, X. Mateos, P. Loiko, K. Yumashev, N. Kuleshov, V. Petrov, U. Griebner, M. Aguiló, and F. Díaz, "Diode-pumped microchip Tm:KLu(WO$_4$)$_2$ laser with more than 3 W of output power," Opt. Lett. **39**(14), 4247–4250 (2014).
26. J. M. Serres, P. Loiko, X. Mateos, K. Yumashev, N. Kuleshov, V. Petrov, U. Griebner, M. Aguiló, and F. Díaz, "Prospects of monoclinic Yb:KLu(WO$_4$)$_2$ crystal for multi-watt microchip lasers," Opt. Mater. Express **5**(3), 661–667 (2015).
27. P. A. Loiko, J. M. Serres, X. Mateos, J. Liu, H. Zhang, A. S. Yasukevich, K. V. Yumashev, V. Petrov, U. Griebner, M. Aguiló, and F. Díaz, "Passive Q-switching of Yb bulk lasers by a graphene saturable absorber," Appl. Phys. B **122**, 105 (2016).
28. V. Petrov, M. C. Pujol, X. Mateos, Ò. Silvestre, S. Rivier, M. Aguiló, R. M. Solé, J. H. Liu, U. Griebner, and F. Díaz, "Growth and properties of KLu(WO$_4$)$_2$, and novel ytterbium and thulium lasers based on this monoclinic crystalline host," Laser Photonics Rev. **1**(2), 179–212 (2007).
29. F. Zhang, S. Han, Y. Liu, Z. Wang, and X. Xu, "Dependence of the saturable absorption of graphene upon excitation photon energy," Appl. Phys. Lett. **106**(9), 091102 (2015).
30. L. C. Kong, G. Q. Xie, P. Yuan, L. J. Qian, S. X. Wang, H. H. Yu, and H. J. Zhang, "Passive Q-switching and Q-switched mode-locking operations of 2 μm Tm:CLNGG laser with MoS$_2$ saturable absorber mirror," Photon. Res. **3**(2), A47–A50 (2015).
31. C. Luan, X. Zhang, J. Zhao, S. Zhao, K. Yang, T. Li, W. Qiao, H. Chu, J. Qiao, J. Wang, L. Zheng, X. Xu, and J. Xu, "High peak power passively Q-switched 2 μm laser with MoS$_2$ saturable absorber," IEEE J. Sel. Top. Quantum Electron. (to be published).
32. T. Lin, H. Sun, X. Wang, D. Mao, Y. Wang, L. Li, and L. Duan, "Passively Q-switched Nd:YAG laser with a MoS$_2$ solution saturable absorber," Laser Phys. Lett. **25**(12), 125805 (2015).
33. P. A. Burns, J. M. Dawes, P. Dekker, J. A. Piper, J. Li, and J. Wang, "Coupled-cavity, single-frequency, tunable cw Yb:YAB yellow microchip laser," Opt. Commun. **207**(1-6), 315–320 (2002).
34. J. Izawa, H. Nakajima, H. Hara, and Y. Arimoto, "A tunable and longitudinal mode oscillation of a Tm,Ho:YLF microchip laser using an external etalon," Opt. Commun. **180**(1-3), 137–140 (2000).
35. J. Saikawa, S. Kurimura, I. Shoji, and T. Taira, "Tunable frequency-doubled Yb:YAG microchip lasers," Opt. Mater. **19**(1), 169–174 (2002).
36. Z. Tian, K. Wu, L. Kong, N. Yang, Y. Wang, R. Chen, W. Hu, J. Xu, and Y. Tang, "Mode-locked thulium fiber laser with MoS$_2$," Laser Phys. Lett. **12**(6), 065104 (2015).
37. H. Xia, H. Li, C. Lan, C. Li, X. Zhang, S. Zhang, and Y. Liu, "Ultrafast erbium-doped fiber laser mode-locked by a CVD-grown molybdenum disulfide (MoS2) saturable absorber," Opt. Express **22**(14), 17341–17348 (2014).

1. Introduction

Transition metal dichalcogenides (TMDs) are materials with chemical formula MX_2 where X = S, Se or Te and M stands for a metal like Mo or W [1]. Bulk TMD materials and, in particular, molybdenum disulphide, MoS_2, are formed of monolayers bound to each other by weak Van-der-Waals forces. In the layers the atoms are strongly bonded by covalent forces [2]. Bulk MoS_2 is hexagonal (2H, space group $P6_3/mmc$, the same as for graphite), with lattice constants $a = 3.16$ Å and $c = 12.29$ Å [2]. Each MoS_2 monolayer is composed of three atomic layers (two layers of S atoms and one layer of Mo in between). Each Mo atom is bonded to six S atoms and each S center is pyramidal and bonded to three Mo atoms. The thickness of a MoS_2 monolayer is ~6.5 Å. Bulk MoS_2 is an indirect bandgap semiconductor ($E_g = 1.23$ eV) while an ideal monolayer is characterized by a direct bandgap of $E_g = 1.8$ eV ($\lambda_g = 690$ nm) [3,4]. However, it is known that the introduction of defects due to a violation of the ideal Mo:S ratio (1:2), in-plane strains or stacking of several monolayers in sheets can strongly affect the band structure of MoS_2 [5,6]. As a result, similar to graphene [7], E_g may reach very small values providing broadband linear absorption in the visible and near-IR [6].

In addition to the broadband absorption, 2D MoS_2 structures exhibit absorption saturation in a broad spectral range from the visible up to ~2.1 μm [6,8,9], similarly to another 2D-materials: graphene [10] and black phosphorus [11]. This effect is related to the finite density of states in the conduction band (CB) in accordance with the Pauli blocking principle, so that at a certain intensity of the incident light, the excitation of carriers from the valence band (VB) to the CB is blocked and bleaching occurs. 2D MoS_2 possesses relative low saturation fluence and ultrafast recovery time of the initial absorption, together with good mechanical properties [8,9]. These properties facilitate the use of 2D MoS_2 structures as nonlinear optical elements (saturable absorbers, SAs) in pulsed (Q-switched and mode-locked) bulk and fiber lasers [6,12,13]. In passively Q-switched (PQS) bulk lasers, MoS_2 SA was exploited in Pr^{3+} (at ~0.6 μm) [14], Yb^{3+} (at ~1 μm) [15,16], Nd^{3+} (at ~1 and ~1.3 μm) [6,17], Tm^{3+} and Ho^{3+} (at ~2–2.1 μm) [6,18] oscillators. However, the achieved pulse characteristics are still inferior compared to lasers PQS by carbon nanostructures (graphene and single-walled carbon nanotubes, SWCNTs) [19–22]. MoS_2 is a “fast” SA and it can produce ns pulses at high repetition rates (ranging from hundreds of kHz potentially up to few MHz), so that it can be an alternative to semiconductor saturable absorber mirrors (SESAMs). In particular, MoS_2 can operate in the spectral range around ~2 μm where the SESAM technology is not mature, while the synthesis of 2D MoS_2 materials is relatively easy. In comparison with graphene, MoS_2 may potentially show higher modulation depth and smaller non-saturable losses, which is crucial for the increase of the pulse energy and shortening of the laser pulses. As compared with SWCNT-based SAs, MoS_2 layers do not require to be embedded into a polymer thin film which can limit the resistance to laser damage.

One way for the ultimate shortening of the laser pulses in PQS oscillators is the use of the microchip design with both gain material and SA placed in a compact plano-plano laser cavity resulting in a short cavity roundtrip time [23]. Low losses inherent to the microchip set-up are also advantageous to increase the laser efficiency and the pulse energy. The use of the microchip concept together with SAs based on graphene and SWCNTs helped to significantly improve the pulse characteristics for PQS lasers [19,21]. In the present work, we report on the first application of few-layer MoS_2 SA in Yb (at ~1 μm) and Tm (at ~1.9 μm) microchip lasers. In the latter case, we show that the MoS_2-based SA performs better compared with its 2D SA counterpart, graphene.

2. Experimental

2.1 Saturable absorber

The saturable absorber was prepared by Pulsed Laser Deposition (PLD) using polycrystalline MoS_2 as a starting material [6]. An optical-grade quartz glass wafer (diameter: 25 mm, thickness: 1.0 mm) was used as a substrate. The MoS_2 target was cold pressed into a 40 mm diameter pellet from the polycrystalline powder. A 248 nm KrF excimer laser (Compex Pro

201, Coherent Inc.) with a pulse duration of 20 ns was used to ablate the target. A pulse energy of 600 mJ, pulse repetition frequency of 5 Hz and a total number of pulses of 300 were used for the deposition. The base pressure of the vacuum chamber raised from ~8.9 × 10^{-5} Pa to 5 × 10^{-4} Pa during the deposition. In order to enhance the uniformity of the film, both target and substrate were rotated, and the substrate temperature was fixed at 300 °C.

The morphology of the synthesized sample was studied by Atomic Force Microscopy revealing a thickness of the MoS_2 film of ~20 nm corresponding to the presence of about ~30 MoS_2 layers if considering an individual layer thickness of ~0.65 nm and their bonding by Van der Waals interaction. The intrinsic transmission of the film was determined as T_0(film) = T(film + substrate)/T(substrate), see Fig. 1(a). The transmission spectra were measured using a Varian CARY-5000 spectrophotometer. A significant rise of absorption below 1 μm is visible which is attributed to scattering loss. The sample shown in the inset of Fig. 1(a) appeared transparent with a slight grey-tint. At ~1.92 μm, T_0 was 95.7% and at ~1.03 μm, it was 91.2%. In the spectrum, a weak and broad band below 1 μm with two poorly resolved peaks at ~400 and 450 nm is observed (marked by # in Fig. 1(a)). These features are typical for defect-free MoS_2 nanosheets and they are related to two (denoted as D and C, respectively) of the four possible electronic inter-band transitions [9]. In dispersed MoS_2, these four transitions are observed at 403, 451, 613 and 674 nm (D, C, B and A transitions, respectively) [9]. Thus, the intense broadband absorption spanning from ~1 up to ~2 μm in Fig. 1(a) cannot be related to the D–A transitions of defect-free MoS_2 nanosheets. As mentioned above, we attribute this absorption to the modification of the band structure of MoS_2 due to defect states, strains and the multi-layered nature of our sample.

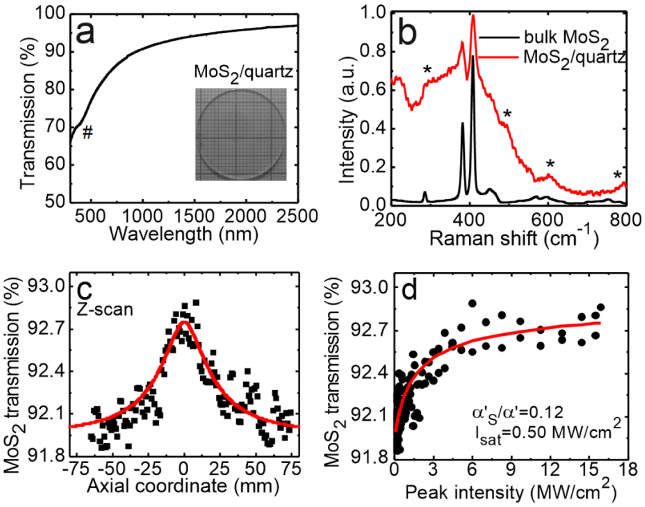

Fig. 1. MoS_2 saturable absorber: intrinsic transmission spectrum, # indicates the D and C electronic inter-band transitions (a), Raman spectrum compared with that of polycrystalline MoS_2, * denotes bands due to the quartz substrate (b), open-aperture Z-scan experiment (c) and the corresponding absorption saturation curve measured at 1.06 μm under ps excitation (d): *points* – experimental data, *red curve* – fitting with Eqs. (1)-(2).

The presence of MoS_2 was confirmed by Raman spectroscopy, Fig. 1(b). The bulk MoS_2 shows four Raman bands at ~34, 286, 383 and 409 cm^{-1} [24]. The vibrational 383 cm^{-1} band (E^1_{2g}) is assigned to the motion of the Mo + S atoms in the *x*-*y* layered plane of the unit cell. The vibrational 409 cm^{-1} band (A_{1g}) is assigned to the motion of the S atoms along the *z* axis of the unit cell. The full width at half maximum (FWHM) of such bands is 7.92 and 7.98 cm^{-1}, respectively [24]. For our MoS_2 film, the E^1_{2g} and A_{1g} bands are clearly observed in the Raman spectrum at 382 and 408 cm^{-1} and the corresponding FWHM of these bands is 15.4 and 13.2 cm^{-1}, respectively. The broadening of the E^1_{2g} band results mainly from the disorder generated in the *x*-*y* layered plane of the material. For the MoS_2 film, a weak and broadband Raman signal at 180-240 cm^{-1} is observed. Its appearance is also related to the presence of defects.

The absorption saturation of the MoS_2-based SA was studied by the Z-scan method. For this measurement, the SA was translated along the focused beam from a pulsed laser providing a variation of the incident laser intensity. By considering spatial and temporal distribution of the laser intensity, the measured intrinsic transmission of the MoS_2 SA is:

$$T_{\text{exp}}(I) = \frac{1}{E}\int_0^{+\infty}\int_0^{2\pi}\int_{-\infty}^{+\infty} T[I(r,t)]I(r,t)rdrd\theta dt, \tag{1}$$

with

$$I(r,t) = I_0 e^{\frac{2r^2}{w_L^2}} e^{-\frac{4\ln 2t^2}{\tau^2}}, \text{where } I_0 = \frac{2E}{\pi w_L^2 \tau *}, \tag{2a}$$

$$\alpha'(I) = \alpha'_{\text{NS}} + \frac{\alpha'_{\text{S}}}{1+(I/I_{\text{sat}})}, \tag{2b}$$

$$\alpha'_0 = 1 - T_0 = \alpha'_{\text{NS}} + \alpha'_{\text{S}}, \tag{2c}$$

where, r and θ are the polar coordinates, t is time, E is the incident pulse energy, I is the incident instantaneous laser intensity, $T(I) = 1 - \alpha'(I)$ is the intensity-dependent transmission of the sample ($\alpha'(I)$ is the intensity-dependent absorption) [6,8], I_0 is the peak on-axis laser intensity, w_L is the radius of the laser beam on the sample (calculated at the $1/e^2$ level, assuming a Gaussian beam profile), $\tau^* \approx 1.06\tau$ is the effective pulse duration (assuming a Gaussian temporal shape of the laser pulses, τ is the pulse duration at the ½ level, e.g. FWHM), I_{sat} is the saturation intensity, α'_S and α'_{NS} are the saturable and non-saturable absorption, respectively, and α'_0 is the initial (small-signal) absorption of the MoS_2-based SA. In Eq. (2)b), the two-photon absorption (TPA) is neglected. As excitation source, we employed a mode-locked Nd-doped laser generating at 1063.6 nm with the following characteristics: $E = 1.12$ nJ, PRF = 58.15 MHz, $\tau = 2$ ps. The laser beam was focused to a spot size of $2w_L = 91.9$ μm corresponding to a Rayleigh length of $z_R = 6.23$ mm. The studied sample was few-layer MoS_2 deposited on a 1 mm-thick quartz substrate. The measured open-aperture Z-scan curve was fitted by using Eqs. (1)-(2) with I_{sat} and α'_S as free parameters. The results are shown in Fig. 1(c),1(d). The Fresnel losses are subtracted. The small-signal absorption of MoS_2 SA is $\alpha'_0 = 8.05\%$ and the best-fitting parameters are $I_{\text{sat}} = 0.50 \pm 0.05$ MW/cm^2 and $\alpha'_S = 0.97 \pm 0.05\%$. Thus, the ratio of the saturable absorption to the small-signal one, $\alpha'_S/\alpha'_0 = 0.12 \pm 0.01$.

For comparison in the PQS laser experiments, a commercial transmission-type graphene-SA was chosen. It consisted of a 1.05 mm-thick fused silica substrate with multi-layer graphene deposited by chemical vapor deposition (CVD). Different layers were deposited subsequently. The intrinsic small-signal transmission T_0 was 94.5% at ~1.92 μm and 93.6% at ~1.03 μm. Thus, the mean number of graphene layers in the sample was $n \approx 2.5$ (between 2 to 3 layers) considering the small-signal absorption of a single layer of carbon atoms being $\alpha'_0 \approx \pi\alpha = 2.3\%$ where $\alpha = e^2/\hbar c \approx 1/137$ is the fine structure constant. The number of carbon layers was further confirmed by Raman spectroscopy, according to the relative intensity of the 2D and G peaks.

2.2 Laser set-up

As laser host material, we used monoclinic $KLu(WO_4)_2$ (shortly KLuW) crystals doped with 3 at.% Yb^{3+} or 5 at.% Tm^{3+} ions. Both laser elements were cut along the N_g optical indicatrix axis of this biaxial crystal since this orientation provides positive thermal lens. The latter is required for the mode stabilization in a plano-plano laser cavity [25,26]. The laser elements were 3.0(*g*) mm thick with an aperture of 3.0(*p*) × 3.0(*m*) mm^2 (*g,p,m*: indices of the KLuW optical indicatrix). Both element faces were polished to laser quality and remained uncoated. They were mounted in a Cu-holder with cooling from all 4 side faces and In foil was used to improve the thermal contact. The holder was water-cooled to 12 °C.

Table 1. Parameters of the Studied Laser Crystals

Crystal	Cut	Doping, at.%	N_{RE}, 10^{20} cm^{-3}	*t*, mm	Aperture, mm^2	λ_p, nm	Abs., %	*M**, m^{-1}/W
Yb:KLuW	N_g-cut	3.0	1.8	3.0	3.0(*p*) × 3.0(*m*)	976	54	2.8_p, 3.5_m
Tm:KLuW	N_g-cut	5.0	3.6	3.0	3.0(*p*) × 3.0(*m*)	805	45	12.9_p, 8.1_m

*Sensitivity factor of the thermal lens; subscript – direction (N_p or N_m-axis) [25,26].

The scheme of the microchip laser set-up is depicted in Fig. 2(a).

The laser cavity consisted of a flat pump mirror (PM) and a flat output coupler (OC). For the Yb-laser, PM was antireflection (AR) coated for 0.78-1.0 μm and high-reflection (HR) coated for 1.02-1.2 μm. For the Tm-laser, it had the same AR-coating but the HR-coating was for 1.8-2.1 μm. The transmission of the OC was T_{OC} = 5% at 1.8-2.1 μm (Tm-laser) or 10% at 1.0-1.2 μm (Yb-laser), which was found to be optimum in our previous experiments with Yb and Tm lasers PQS by a single-layer graphene SA [19,27]. The transmission-type SA (based on $\mathrm{MoS_2}$ or graphene) was placed between the crystal and the OC and it was in a mechanical contact with both optical elements. Thus, the total geometrical cavity length was equal to the sum of the lengths of the laser element and the SA (~4 mm).

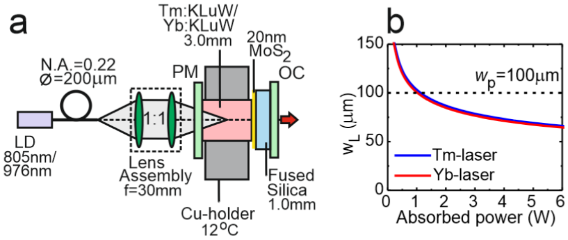

Fig. 2. (a) Scheme of the Yb and Tm microchip lasers PQS by a $\mathrm{MoS_2}$-based SA: LD – laser diode, PM – pump mirror, OC – output coupler; (b) calculated mean radius of the laser mode w_L(SA) in the SA versus the absorbed pump power for Yb and Tm lasers (w_p: pump spot radius).

The laser element was pumped through the PM by a fiber-coupled InGaAs or AlGaAs laser diode emitting at ~976 nm or at ~805 nm, respectively (both unpolarized). This corresponded to the excitation of the $^2\mathrm{F}_{7/2} \rightarrow {}^2\mathrm{F}_{5/2}$ or $^3\mathrm{H}_6 \rightarrow {}^3\mathrm{F}_4$ transitions of Yb^{3+} and Tm^{3+} ions, respectively. The fiber parameters for both pump diodes were: N.A.: 0.22 and core diameter: 200 μm. The pump light was reimaged by a lens assembly (reimaging ratio: 1:1, focal length: 30 mm) providing a mean pump spot radius of w_p = 100 μm and a confocal parameter of the pump beam of $2z_\mathrm{R}$ = 1.7 mm for both diodes. The M^2 parameter of the pump beam was ~71 and ~86 for the InGaAs and AlGaAs diodes, respectively. The Tm laser was single-pass pumped whereas pumping the Yb-laser was consideres as double-pass pumping due to partial reflection of the pump on the OC (~90%). The total absorption of the pump light for the Yb:KLuW and Tm:KLuW crystals amounted to 54% and 45%, respectively (under lasing conditions).

The radii of the laser modes w_L in the crystals and on the SAs were calculated with the ABCD-method using the parameters of the thermal lens in Yb: and Tm:KLuW crystals [25,26], see Fig. 2(b). The thermal lens was described as a thin lens located in the center of the crystal. The value of w_L decreases from 85 to 65 μm (assuming M^2 = 1) when the absorbed pump power P_{abs} varies from 2 to 6 W and it is very close for both lasers although the thermal lens in Tm:KLuW crystal is much stronger. This difference is compensated by the almost 2 times longer laser wavelength of the Tm-laser, as compared with the Yb-doped one.

A fast InGaAs photodiode with 200 ps rise time (Alphalas, model UPD-5N-IR2-P), and a 2 GHz digital oscilloscope (Tektronix DPO5204B) were used for detection of the Q-switched pulses.

3. Experimental results

3.1 Tm laser

At first, we studied the continuous-wave (CW) performance of the Tm-laser when removing the SA from the cavity but keeping the same total cavity length. The maximum P_{abs} was limited to 4.9 W in order to avoid thermal fracture of the crystal. The Tm:KLuW laser generated 1.57 W at λ_L = 1927–1948 nm (multi-peak spectrum) with a slope efficiency of η = 51% with respect to the absorbed pump power and the laser threshold was at 1.8 W, see Fig. 3. The laser emission was linearly polarized ($E \parallel N_m$, which is in agreement with the gain spectra [28]).

Stable Q-switching was achieved with both SAs, MoS_2 and graphene. For the Tm-laser PQS with MoS_2-based SA, the maximum average output power reached 1.27 W at λ_L = 1929 nm corresponding to η = 43%, see Fig. 3. The conversion efficiency with respect to the CW mode was as high as η_{conv} = 81% and the threshold was at P_{abs} = 2.15 W. When inserting the graphene-SA, the laser generated 1.03 W at a shorter wavelength, 1926 nm, corresponding to lower η = 39% and η_{conv} = 67%. The laser threshold was at 2.3 W. Shortening of the laser wavelength for PQS lasers with respect to the CW operation mode, Fig. 3(b), is related to increased intracavity losses caused mainly by the non-saturable losses (α'_{NS}) of the SA. By analyzing η_{conv} and λ_L for both SAs, we have to conclude that multi-layered graphene has higher non-saturable loss at ~2 µm. For both SAs, the laser output was linearly polarized, $E \parallel N_m$.

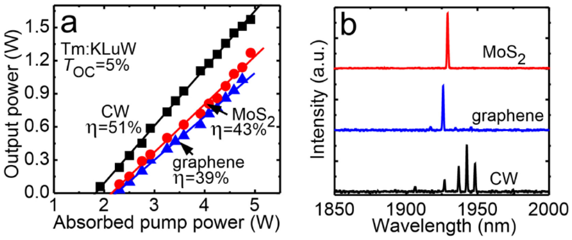

Fig. 3. Tm:KLuW laser PQS with MoS_2- and graphene-based SAs and in CW for comparison: input-output dependences, η is the slope efficiency (a), and typical laser emission spectra at P_{abs} = 4.8 W (b).

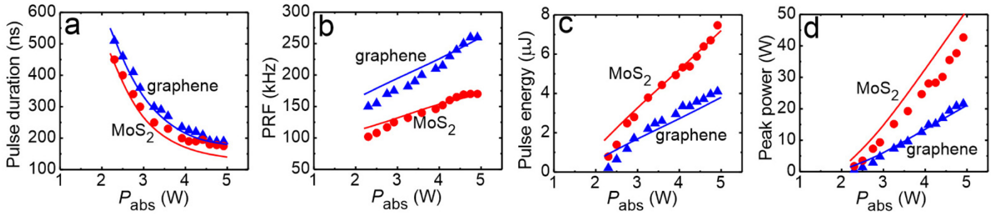

Fig. 4. Tm:KLuW laser PQS with MoS_2- and graphene-based SAs: (a) pulse duration, τ, (FWHM), (b) pulse repetition frequency (PRF), (c) pulse energy, $E_{out} = P_{out}$/PRF, and (d) peak power, $P_{peak} = E_{out}/\tau$, *symbols* – experimental data, *curves* – numerical modeling.

The pulse characteristics of the PQS Tm-laser show strong dependence on P_{abs}, Fig. 4 that is typical for "fast" SAs. For "slow" SAs, under the conditions of single-pulse generation, the pulse duration and energy are weaker dependent on P_{abs} as they are determined by the cavity parameters and the spectroscopic properties of the laser material/SA). For MoS_2-SA, with the increase of P_{abs}, the pulse duration τ decreased from 450 to 175 ns and the PRF increased nearly linear from 102 to 170 kHz. According to these results, we calculated the pulse energy ($E_{out} = P_{out}/PRF$) and peak power ($P_{peak} = E_{out}/\tau$) which reached 7.5 μJ and 42.8 W at P_{abs} = 4.8 W, respectively. When using graphene-SA, the pulse durations were similar, ranging from 510 to 190 ns while the PRF was almost twice higher, ranging from 150 to 260 kHz. This increase led to lower maximum E_{out} = 4.1 μJ and P_{peak} = 22 W.

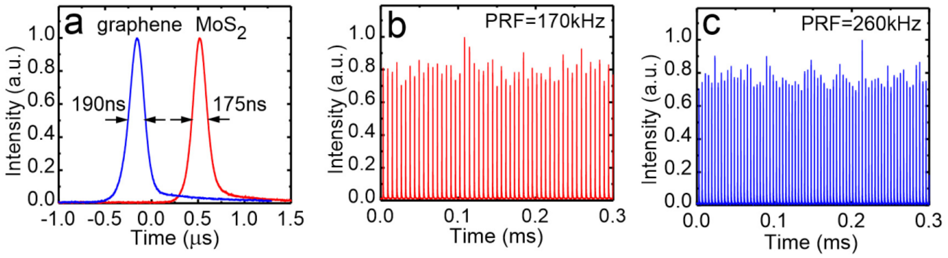

Fig. 5. Tm:KLuW laser PQS with MoS_2- and graphene-based SAs: (a) oscilloscope traces of the shortest pulses and the corresponding pulse trains measured at P_{abs} = 4.8 W for MoS_2- (b) and graphene-SA (c).

The oscilloscope traces of the shortest single Q-switched pulses achieved in the Tm-laser are shown in Fig. 5(a). The pulses exhibit nearly Gaussian temporal shape and no CW pedestal is observed. The corresponding pulse trains for the MoS_2- and graphene-based SA are shown in Figs. 5(b),5(c). The intensity instabilities in the pulse trains are <15% and the rms pulse-to-pulse timing jitter (the deviation of the pulse-to-pulse separation from the average pulse period) was ~7%; both values were similar for the MoS_2- and graphene-SA. These instabilities are attributed to heating of the SA by the residual non-absorbed pump by the laser crystal [19]. The latter could be avoided with a proper coating on the crystal end-face. Stable PQS operation of the Tm:KLuW/MoS_2 laser has been achieved for tens of min.

No damage of the MoS_2-SA was observed in our experiments, which allows us to estimate the laser-induced damage threshold (LIDT) as at least 30 MW/cm^2 for ns-pulses (as it follows from the calculation of the peak intracavity intensity for the Tm-laser).

3.2 Yb laser

The CW and PQS performance of the Yb-laser is analyzed in Fig. 6. For the Yb-laser, stable PQS was achieved for P_{abs} < 5.5 W; at higher absorbed pump powers, a multi-pulse behavior with a significant timing jitter was observed. The CW Yb:KLuW laser generated 0.93 W at 1046–1048 nm with η = 32% and the laser threshold was at P_{abs} = 2.4 W. For the MoS_2-SA PQS Yb-laser, the maximum average output power was 147 mW at 1030 nm corresponding to η = 7% and η_{conv} = 16%, Fig. 6. The laser threshold was at P_{abs} = 3.4 W. When using graphene-SA, the output characteristics were better as compared with those for MoS_2-SA but still poor as compared with the CW performance. The Yb-laser PQS with graphene-SA generated 315 mW at 1032 nm with higher η = 12% and η_{conv} = 34%, and lower laser threshold, observed at 2.7 W. For both CW and PQS operation modes, the output from the Yb-laser was linearly polarized, $E \parallel N_m$, which is also in agreement with the gain anisotropy [28]. By comparing Fig. 3(a) and Fig. 6(a), one can conclude that MoS_2-SA possesses higher non-saturable loss at ~1 μm as compared to graphene and that both SA materials exhibit higher losses at ~1 μm compared to ~2 μm.

The pulse characteristics of the Yb-laser show similar dependences on the absorbed pump power as in the case of the Tm-laser, Fig. 7. The pulse duration decreased from 740 to 140 ns and from 670 to 220 ns and the PRF increased from 170 to 320 kHz and from 125 to 300 kHz for the graphene-SA and the MoS_2-SA, respectively. However, the deteriorated output laser performance led to relatively low pulse energies and, consequently, also to low peak powers.

These two parameters reached 0.5 μJ and 2.2 W for MoS_2-SA and 1.0 μJ and 7.0 W for graphene-SA.

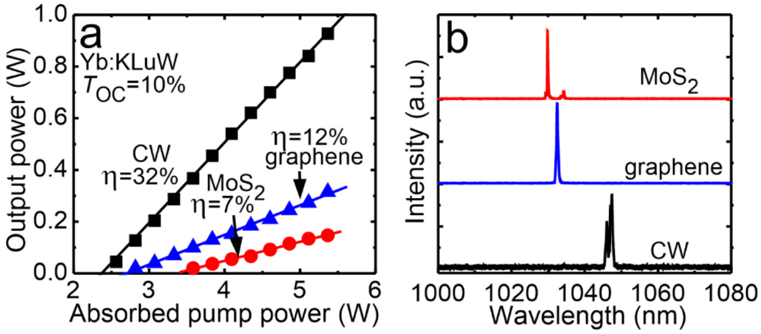

Fig. 6. Yb:KLuW laser PQS with MoS_2- and graphene-based SAs and in CW for comparison: input-output dependences, η is the slope efficiency (a), and typical laser emission spectra at P_{abs} = 5.4 W (b).

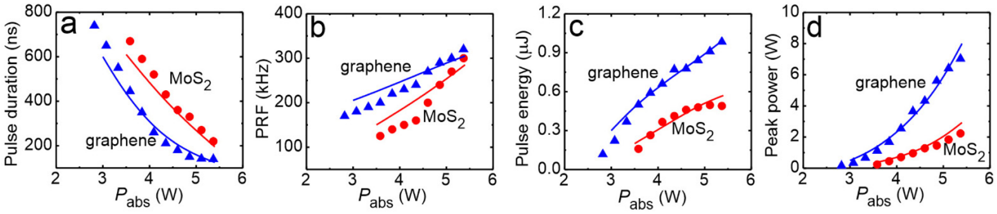

Fig. 7. Yb:KLuW laser PQS with MoS_2- and graphene-based SAs: (a) pulse duration, (b) PRF, (c) pulse energy and (d) peak power, *symbols* – experimental data, *curves* – numerical modeling.

The oscilloscope traces of the shortest single Q-switched pulses and the corresponding pulse trains for the Yb-laser are shown in Fig. 8. The temporal shape of the single pulses is slightly asymmetric and the intensity instabilities in the pulse trains are much higher (~25%) than in the case of the Tm-laser (compare Fig. 5(b),5(c)). The rms pulse-to-pulse timing jitter is also higher, ~15%. These instabilities, the low Q-switching conversion efficiency η_{conv} and the existence of an upper limit for stable Q-switching indicate higher non-saturable loss of both SAs and, hence, stronger detrimental effect of its heating.

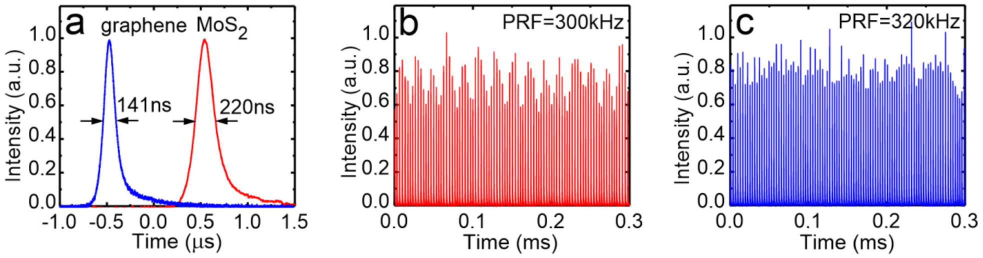

Fig. 8. Yb:KLuW laser PQS with MoS_2- and graphene-based SAs: (a) oscilloscope traces of the shortest pulses and the corresponding pulse trains measured at P_{abs} = 5.4 W for MoS2- (b) and graphene- (c) SA.

A summary of the output characteristics of the Yb and Tm lasers PQS with MoS_2- and graphene-based SAs is presented in Table 2.

Table 2. Output characteristics of Yb: and Tm:KLuW microchip lasers PQS with MoS_2 and graphene SAs

Crystal	SA	P_{out}, mW	η, %	λ_L, nm	τ, ns	PRF, kHz	E_{out}, μJ	P_{peak}, W
Tm:KLuW	MoS_2	1270	43	1929	175	170	7.5	42.8
	graphene	1030	39	1926	190	260	4.0	20.9
Yb:KLuW	MoS_2	147	7	1030	220	300	0.5	2.2
	graphene	315	12	1032	140	320	1.0	7.0

4. Discussion

In order to explain the significant difference in the performance of Yb and Tm lasers PQS by MoS_2 and graphene-based SAs, we simulated the pulse characteristics of the two lasers within the model of a quasi-three-level medium and a "fast" SA, see details in [27]. The spectroscopic properties of Yb^{3+} and Tm^{3+} ions in KLuW used for the modeling can be found elsewhere [28]. The results are shown in Fig. 4 (Tm-laser) and Fig. 7 (Yb-laser) as solid curves. The computations are in good agreement with the experimental data and they correctly predicts the dependence of the pulse characteristics on P_{abs}, namely, the shortening of τ and the increase of E_{out} with P_{abs}, both showing some saturation at high pump levels, as well as a nearly linear increase of the PRF. From the modeling, we estimated the absorption saturation characteristics of both SAs, namely I^*_{sat} and α'_S (the small-signal absorption, α'_0, is unambiguously determined from the absorption spectra). The results are shown in Table 3. In the model, the intracavity laser intensity was defined as peak on-axis one and thus I^*_{sat} extracted from the fitting can differ from the value determined from z-scan measurement (see e.g. Figure 1(c,d)). However, such a modeling allows for comparison of nonlinear characteristics of both studied SAs at ~1 μm and ~2 μm.

Table 3. Saturable absorption properties* of MoS_2 and graphene-based SAs

SA	λ, μm	I^*_{sat}, MW/cm^2	α'_S, %	α'_0, %	α'_S/α'_0
graphene	~1	1.0 ± 0.2	0.22 ± 0.02	6.4	~0.034
	~2	0.6 ± 0.2	0.23 ± 0.02	5.5	~0.042
MoS_2	~1	0.8 ± 0.3	0.28 ± 0.03	8.8	~0.032
	~2	0.5 ± 0.2	0.32 ± 0.03	4.3	~0.074

*Estimated from the modeling of output characteristics of Yb and Tm lasers PQS with these SAs.

From Table 3, we conclude that much better performance of the PQS lasers at ~2 μm is related to lower saturation intensity I_{sat} and a higher fraction of the saturable loss, α'_S/α'_0, at this wavelength. This statement holds true for both SAs. For graphene, the tendency for the increase of I_{sat} with the photon energy $h\nu$ is well-known [29] and it is related to the mechanism of saturation of this almost zero bandgap material: when working with higher $h\nu$, more electrons from the VB are needed to be excited into the CB in order to reach optical bleaching. Because MoS_2 is a similar 2D material, we can expect a similar decrease of I_{sat} at longer wavelengths (lower $h\nu$). Regarding the increase of α'_S/α'_0 with the wavelength, it can also be understood if considering that the scattering losses decrease fast with λ, e.g. as described by an empirical formula for the Mie scattering, $\sim\lambda^{-2.35}$ [9].

If we compare the behavior of graphene and MoS_2-SAs the saturation intensity for these two SAs is rather similar (cf. Table 3). At ~2 μm, MoS_2-SA offers higher modulation depth (α'_S = 0.32%) and lower non-saturable loss (α'_{NS} ~4.0%) compared with graphene. As a consequence, this leads to a much higher pulse energy and better Q-switching conversion efficiency η_{conv} observed in the Tm-laser. At ~1 μm, the non-saturable loss in MoS_2-SA (α'_{NS} ~8.5%) is increasing much faster than for graphene-SA while the modulation depth for the two SAs is very similar (α'_S ~0.2%). Consequently, at ~1 μm, a better performance of the Yb-laser is expected when using graphene-SA.

Comparing the results of the present work with those previously reported for near-IR bulk lasers PQS with MoS_2-SA, see Table 4, to date, MoS_2 has been applied for PQS of bulk lasers at ~1 μm (based on the Yb^{3+} and Nd^{3+} ions) and at ~2 μm (based on the Tm^{3+} and Ho^{3+} ions). At ~1 μm, the use of MoS_2 resulted in relatively low E_{out}, typically not exceeding 1 μJ, and pulse durations of few hundreds of ns similar to our results. At ~2 μm, slightly higher pulse energies (few μJ) were achieved still at relatively long pulse durations. As a result, the peak power extracted from MoS_2-SA PQS lasers was limited to few watts. The characteristics achieved in the present work for Tm:KLuW laser PQS with MoS_2 are superior with respect to all previous publications in terms of pulse energy and duration (and, in consequence, peak power that reached >40 W), and also in terms of power scaling because >1 W of average output power was extracted.

Table 4. Parameters of near-IR bulk lasers PQS with MoS_2-based SA reported so far

Ion	Crystal	P_{out}, mW	η, %	τ, ns	E_{out}, μJ	P_{peak}, W	Ref.
Tm^{3+}	KLuW	**1270**	**43**	**175**	**7.5**	**42.8**	This work
	CLNGG	62	-	4840	0.72	0.2	[30]
	$GdVO_4$	100	7.3	800	2.1	2.6	[18]
Tm^{3+}/Ho^{3+}	YGG	206	-	410	1.38	3.4	[6]
	YAP	270	5	435	4.9	11.3	[31]
Yb^{3+}	KLuW	147	7	220	0.5	2.2	This work
	LGGG	600	24	182	1.8	9.9	[16]
	CYB	105	-	420	0.75	1.8	[15]
Nd^{3+}	$GdVO_4$	227	-	970	0.31	0.3	[6]
	YGG	52	-	729	0.67	0.9	[6]
	YAP	260	11	227	1.11	4.9	[17]
	YAG	24	-	2800	1.2	0.4	[32]

According to the modeling of the MoS_2 PQS Tm lasers, we expect that scaling of the pulse energy up to few tens of μJ and shortening of the pulse duration to few ns may be achieved by using (i) higher modulation depth of the MoS_2-SA and (ii) gain materials with longer storage times, e.g. Tm^{3+}-doped fluorides. In this way, a peak power from this type of lasers could reach few kW.

Tunable laser sources are of interest for applications in spectroscopy, remote sensing and medicine, as one can adjust the laser wavelength to match exactly, e.g., the absorption line of a certain molecule for its detection (e.g., H_2O), or to vary the penetration depth of the laser radiation into a certain material, e.g. a biological tissue. For Yb:KLuW and Tm:KLuW lasers, tuning of the laser emission in the 1.0-1.05 μm and 1.81-1.99 μm ranges, respectively, is possible [28]. Tuning of microchip lasers is more difficult as compared to long cavity lasers where a birefringent filter can be used. It may be realized (i) by temperature-variation of the air gaps between the optical components of the cavity [33], (ii) by using an external etalon [34] or (iii) by placing the microchip in a secondary Z-shaped cavity [35]. Further work on tuning of the Tm:KLuW/MoS_2 microchips can be done by using one of these approaches.

The characteristics of the studied MoS_2-SA make it promising for possible applications in mode-locked (ML) lasers. To date, mode-locking with MoS_2-SA has been demonstrated for Yb, Er and Tm fiber lasers [13,36,37] and Q-switched mode-locking – for a Tm bulk laser [30]. The utilization of MoS_2-SA in bulk continuous-wave ML lasers may be successful after optimization of the synthesis method for SA resulting in better optical homogeneity and reduced non-saturable losses.

Further work on PQS 2 μm microchip lasers may focus on the comparison of the known 2D material-based SAs, e.g. graphene, MoS_2, WS_2, black phosphorus (BP), and topological insulators based on Bi_2Se_3, Bi_2Te_3 or Sb_2Te_3. In particular, few-layer BP may be promising particularly at long wavelengths (~2 μm, or ~0.6 eV) due to the relatively narrow direct energy band-gap, ~0.3 eV [11].

5. Conclusion

In conclusion, we have successfully applied a MoS_2-SA for passive Q-switching of Yb and Tm microchip lasers, for the first time to the best of our knowledge. The Tm-laser generated 175 ns / 7.5 μJ pulses at a repetition frequency of 170 kHz and the average output power exceeded 1 W with 43% slope efficiency which represents a significant improvement with respect to graphene PQS microchip lasers (cf. Table 4 and Ref [19].). Taking into account the broadband absorption of MoS_2 and the relatively simple fabrication method, it can be considered as a promising “fast” SA for the ~2 μm spectral range potentially capable of generating few ns pulses at PRFs in the MHz-range. In addition, it can be considered as a potential alternative to SESAMs whose technology at ~2 μm is still far from being mature. The required improvements in the synthesis technology of MoS_2 SA are related to the reduction of the scattering losses (which will further increase the α'_S/α'_0 ratio) by depositing highly uniform and large-area films, and by precise control of the film thickness. This may lead to the scaling of the pulse energy and improvement of the long-term stability of the PQS operation. The direct deposition of MoS_2 on a crystal end face may further reduce the pulse duration by shortening of the cavity length (i.e. reduction of the cavity round-trip time). However, the potential of MoS_2 for PQS at ~1 μm seems to be very limited because it cannot compete with the well-developed “fast” SAs in this spectral range.

Acknowledgments

This work was supported by the Spanish Government under projects MAT2013-47395-C4-4-R and TEC2014-55948-R, and by the Generalitat de Catalunya under project 2014SGR1358. F.D. acknowledges additional support through the ICREA academia award 2010ICREA-02 for excellence in research. This work has received funding from the European Union's Horizon 2020 research and innovation programme under grant agreement No 654148 Laserlab-Europe and under the Marie Skłodowska-Curie grant agreement No 657630.